Proceedings of the Fifth (1995) International Offshore and Polar Engineering Conference
The Hague, The Netherlands, June 11-16, 1995

ISBN 1-880653-16-8 (Set); ISBN 1-880653-18-4 (Vol II)

Steel Catenary Risers for Deep Water Applications

C.P. Pesce, J.A.P. Aranha, C.A. Martins and M.O. Pinto
Escola Politécnica da Universidade de Sao Paulo
Brazil

ABSTRACT

Steel catenary risers connected to floating production systems of semi-submersible type in deep water have been analysed. Static and dynamic response calculation to extreme loading conditions as well fatigue life predictions indicate that, in many cases, a proper configuration can be found in order to comply with design criteria. This paper deals with design procedures and modeling, pointing out a number of uncertainties that deserve special consideration. In particular, dynamic bending stresses in the touch-down region are of special concern, as results from existing computer codes can be significantly affected by discretization and boundary conditions modeling. It has been found that slow drift-oscillations of the vessel and wave frequency motions imposed to the top end of the riser are, in general, the primary cause of fatigue damage. Vortex induced vibrations can play a rule as well, depending on depth, current profile and geometrical properties of the riser.
Keywords: Steel Catenary Risers, riser dynamics, fatigue, floating production systems, asymptotic analysis, Touchdown Point.

1. INTRODUCTION

Steel Catenary Risers (SCR) is, in fact, a design concept yet to be proved as a satisfactory one. A number of advantages can be pointed out, if compared to standard solutions as flexible risers or tensioned risers. As mentioned by Phifer et al (1994), subsea connections and heave-compensator are no longer needed. Another obvious advantage is lower cost. Larger diameters could also be argued as an advantage over flexible pipes. On the other hand, installation procedure tends to be more complex and, not so obvious, design efforts are required to be more extensive, at least at this moment. This is easy to explain, since for a SCR the *touch down point* (TDP) is definitely a "hot spot," under either extreme load conditions or fatigue considerations.

As will be seen through the next sections, the dynamic bending moment near the TDP is responsible for both extreme stresses and cyclic stresses that lead to fatigue. Concerning this particular phenomenon, as usual S-N curves follow exponential laws, any small error in the bending moment gives rise to a poor estimate for the damage. The precise evaluation of curvature near the TDP is then a strong requirement for the designer. However, existing numerical methods and codes for predicting dynamics of catenary risers give some "scattered" results for the dynamic curvature at the TDP, as shown in Aranha, Martins & Pesce, 1995, where asymptotics and boundary-layer thechniques are put together in developing some analytical tools. Here, differently from the TLP case, (see Phifer et al (1994)), if a Semi-Submersible platform is used as the Floating Production System (FPS), the SCR will be subjected to rather severe dynamic loading, imposed to the top through motions in the wave-frequency range . In order to comply with design criteria for maximum stresses in extreme environmental conditions and also concerning fatigue due to bending, the designer is now forced to define a neutral configuration (no environmental loads) characterized by a rather larger angle with the vertical at the top. This fact implies in larger values for the tension (modifying the mooring system response) as well as in smaller curvatures at TDP. Implies also in a non-neglectable variation of the TDP position during slow-drift oscillations, amplifying dramatically the accumulated damage due to this kind of loading. On the other hand, if angle at top is increased, severe environmental conditions can give rise to large dynamic tension along the riser, and *eventually to compression*, if further offset positions are concerned. As it can be seen, designing a SCR for a FPS of semi-submersible type in deep water applications, is a matter of balancing conflicting dynamic responses and behaviors, convergence of which being not assured even if an iterative design procedure approach is applied.

Definition of balanced design criteria, comprehending items as maximum permitted excursion for the FPS, maximum permitted accumulated damage, maximum stresses in extreme conditions, stress concentration factors to be used, etc., is now of special concern.

Vortex Induced Vibrations (VIV), by its turn, was found to be of minor importance, concerning fatigue life evaluation. However, as existing methods of evaluation of VIV response (mostly based in the works of Iwan & Blevins, 1974, Iwan, 1975, 81 and Lyons & Patel, 1986) were formerly developed for circular tubes subjected to flows at right angles, caution must be taken in extracting any conclusion, even if such models are adapted accordingly, as the one used in this work.

The present paper aims to discuss some of these important points, illustrating them with examples extracted from preliminary case studies performed for Campos Basin, Brazil. Installation will not be addressed. Section 2 presents a general design & analysis procedure, illustrated by a flowchart and corresponding design spiral. Section 3 discusses on dynamics as well as on modelling. Section 4 presents some numerical examples. Section 5, besides conclusions, raises some later questions. Vortex Induced Vibrations are addressed in Appendix A.

2. DESIGN & ANALYSIS

Figure 1 presents a somewhat standard riser design flowchart. Figure 2 shows the corresponding "design spiral". Analytical tools are refined as the design spiral is followed.

We focus attention on steps 1 to 6, mainly on topics 2, 3 and 4. A brief discussion is made. Modeling techniques and tools are addressed in section 3.

We suppose to be known the following data:

- *characteristics of the site:* position, depth, platform location and orientation, type of soil, bottom profile, etc.
- *statistical representation of environmental conditions:* waves (spectra distribution), current profiles (direction included), wind.
- *riser functional characteristics:* type of hydrocarbon, work pressure and flow, etc.
- *FPS general data and response curves:* frequency response to waves, mooring system static and dynamic (slow-drift) response, wind and current drag curves, etc.
- *general design criteria:* maximum value for the top end tension, desired range for riser angle at top, geometric and operational restrictions, desired fatigue life, strength safety margins, etc.

We suppose also that installation procedures can always be specified accordingly.

Step 1 - General Specification

The first task comprises elementary calculations in order to define diameter and thickness. Maximum values for the top end tension, buckling strength to external pressure, corrosion thickness margin, hydrostatic stability (immersed net weigth), are some of the requirements that must be achieved. Von Mises criterion is usually applied for stress evaluation.

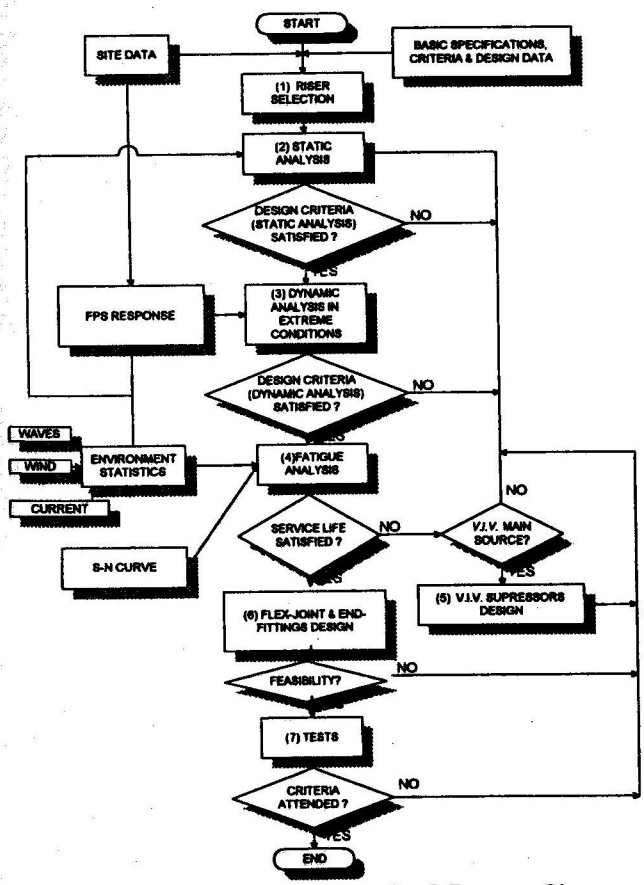

Figure 1. ***Design Flowchart for a Steel Catenary Riser***

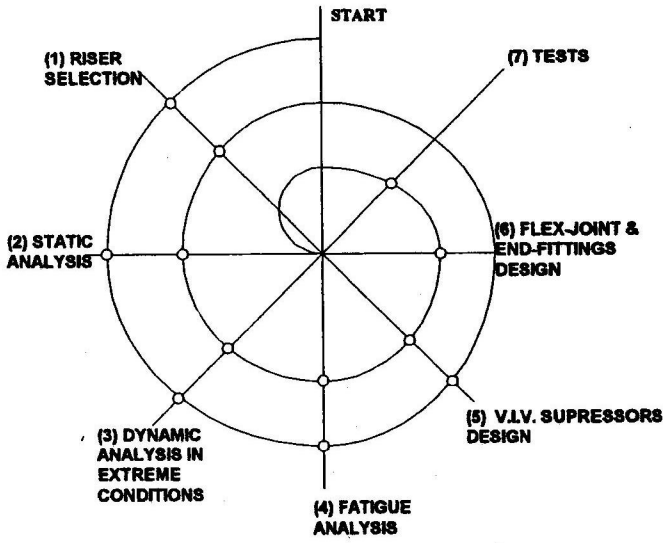

Figure 2. ***Design Spiral for a SCR***

Step 2 - Static Analysis

This second task aims to define the total length for the line, thus specifying the neutral configuration. Static analysis is repeated untill a satisfactory length is obtained. A simple procedure oriented to minimize top end tension can be followed:

- a structural safety margin, accounting for the maximum dynamic overloading is established (2 has proved to be a good value for SCRs in deep water);
- iteratively running a standard static analysis program code, the longest riser length is determined such that, in the nearest FPS offset (dependent on mooring system design and usually defined as a percentage of depth), corresponding to extreme environmental conditions, the maximum stress value computed on the riser (close to the TDP) is less than the assumed safety margin.;
- static analysis is then run for the furthest FPS offset; if maximum top end tension is greater than the allowed value we go back to step 1.

Step 3 - Dynamic Analysis in Extreme Environmental Conditions

In the third task a number of extreme loading conditions are imposed to the FPS, according to the statistical data available for the field. Usually, two different combinations are used, namely centenary-wave/decenary-current and vice-versa, both imposed toward either the "near FPS offset" direction or the "far FPS offset" one. To the centenary wave combination generally correspond the largest loads, as FPS first-order motions are the main loading source. If stress values on the hot-spots (TDP or top end) overcomes the allowable ones (usually circa 70-80% of yield stress), step 2 is addressed again, in order to redefine the neutral configuration properly. The same must be done if dynamic compression (negative effective tension) comes out in some part of the riser, usually close to the TDP. In such a situation slacking is likely to occur, giving rise to a strong non-linear behavior, resulting in large values for the bending moment. As it is shown in Aranha, Martins & Pesce (1995), dynamic curvature near the TDP is proportional to dynamic tension, and in opposite phase.

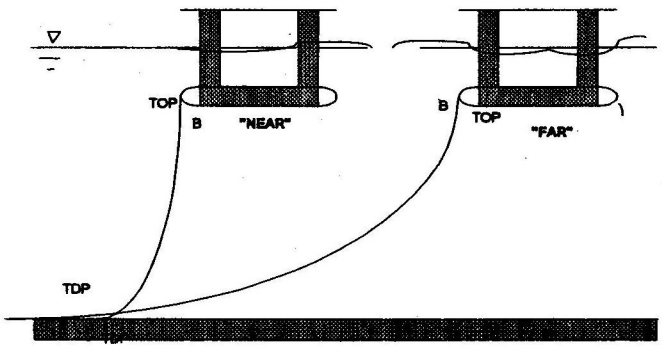

Figure 3. *FPS Offset Positions*

Notice also that, during this step, riser response in damaged mooring conditions must be verified. A somewhat conservative assumption is to run the dynamic analysis around the maximum offset that occurs after the mooring system fails. In such situations allowing stress values to reach 100% of yield stress sounds as a reasonable criterion. However, it seems questionable for these authors if some small amount of dynamic compression should be tolerated near the TDP in damaged mooring conditions, even if the non-linear simulation program code used presents a good numerical behavior in this kind of situation.

The use of a frequency domain response model, can be extremely helpful as an additional tool, saving a large amount of computing time in this step. and permitting to envisage compression. A pinned boundary condition for the TDP is correct to leading-order in $(v/c_0)^2$ (usually a small quantity), where v is the typical value for the TDP variation speed and c_0 is the propagation velocity of transverse waves (see section 3).

Step 4 - Fatigue Analysis

Three are the main sources of fatigue:

- motions in the wave-frequency range (first-order), imposed to the top by FPS and by direct wave action along the riser span;
- slow-drift motions imposed to the top by FPS;
- vortex induced vibrations.

For each condition (wave, current, wind) chosen to be representative of the site environment, and so for each corresponding FPS offset, we then calculate the accumulated damage per year, by applying a standard S-N curve and Palmgren-Miner Law. Fatigue sources are supposed simultaneous but, otherwise, independent of each other.

Weighting the various computed damage values by the probability of occurrence of each selected environmental condition the total damage accumulated per year is computed and fatigue life calculated. If fatigue life is less than expected life, we go back to step 2. Expected life is usually assumed to be ten times design life (corresponding to a maximum accumulated damage value of 10%). Notice that frequency-domain models are, once more, extremely useful in the former cycles of design.

Step 5 - VIV Suppressors Design

If, during the former cycles of design, VIV shows up as a primary source of fatigue, suppressors must be designed. Even if standard concepts are chosen, tests must be carried out in order to quantify the device efficiency. Helical strakes, for instance, must have the optimum pitch determined. We go back to step 2 again, as this kind of device alters the hydrodynamic forces applied to the riser.

Step 6 - Flexible Joints

As it will be seen later, the effect of flexible joints is local, the global configuration and behavior of the riser being governed mostly by catenary dynamics. Neverthless, the average and dynamic values of curvature and angle at the very top are significantly affected. Usually, a properly defined flexural spring is applied as boundary condition, as static and dynamic analysis are performed. This spring is linear if a frequency-domain model is run, what is usually done during the former iterations, and nonlinear, if a time-domain solution is undertaken. A technique that deserves some discussion consists in performing the analysis under a simple pinned boundary condition at top, correcting the values of curvature and angle by means of an asymptotic model (see section 3.1).

Once a proper flexural curve is found for the joint, under which the required top angle range, allowed stress value and expected fatigue life are satisfied, the flexible joint is then designed.

Step 7 - Testing

As SCR is a new concept, testing is crucial, at least at present. The tests can be divided in three types:

- prototype tests;
- model-scale tests;
- full-scale measurements.

In the former category weld fatigue is of primary concern, as reported in Phifer et al, 1994. Standard fatigue testing on full-size weld specimens can be performed for the proper S-N curve selection, although API X' type has shown to be adequate (Phifer et al., 1994).

Flexible-joint performance is the second item to be addressed in the prototype tests. As shown in Phifer et al, however, reliability can be assumed, concerning fatigue, leakage and elastomer integrity.

Model-scale tests should be run in order to:

- verify dynamic response to extreme-loading conditions (curvature at TDP, Tension and angle at top, compression along the riser, etc.);
- optimize VIVsuppressors.

Ful-scale measurements should be planned in order to verify static as well as dynamic response of the riser. Tension, curvature and angle at top, curvature and tension at TDP are of major concern. Waves, wind and current profile as well as first-order and slow-drift motions at the top end are input variables that must be accurately measured.

3. DYNAMICS AND MODELING

Before going on with analysis and design procedures, a brief overview on the main aspects of riser dynamics seems to be convenient. Three main topics will be addressed:

- the local nature of flexural rigidity effects near TDP and flexible-joint at top end;
- boundary condition at TDP;
- dynamic curvature in the vicinity of TDP;

The results presented and discussed hereinafter are mostly extracted from Aranha, Martins & Pesce, 1995. The mentioned paper focuses attention on two-dimensional riser dynamics, by means of asymptotic and local analysis, enlarging concepts firstly addressed by Triantafyllou et al (1985). The main conclusions are summarized below for free-hanging "catenary" risers.

Another important topic, Vortex Induced Vibrations (VIV) concerning fatigue, is treated in the Appendix A.

3.1 Local Nature of Flexural Rigidity Effects in the Vicinity of Points of High Curvature

Flexural rigidity has only a local effect either on static or dynamic response, being restricted to the vicinity of points presenting a high value for the static curvature, or to points subject to a large variation on curvature, usually near the TDP and to the flexible-joint, at top end. Such a region has a typical length scale - that we have called "flexural length" - given by $\lambda = \sqrt{EJ/T_0}$, where EJ is the flexural rigidity and T_0 is the static tension near the considered point. If a typical SCR (external diameter of 10") in 1000m deep water is taken as an example, we get for the parameter λ, in the TDP vicinity, values around 10 meters. Such a value depends, of course, on FPS offset. Far away from this point ($s/\lambda >> 1$, where s is the arch-length coordinate, measured from TDP), bending stiffness plays no important role, static configuration and dynamic response being dominated by the classical catenary equations. Let then $\chi_0(s) = d\theta_0/ds$ be the exact catenary curvature ($EJ = 0$). By applying standard "boundary-layer techniques" and local analysis, the following result, concerning the static curvature close to the TDP, can be derived (Aranha et al, 1995),

$$\chi_{f,0}(s) = H(s+\lambda)(1-e^{-(s+\lambda)/\lambda})\chi_0(s) \quad , \quad (1)$$

where $H(s+\lambda)$ is the Heavyside Function.

Notice that the curvature of a catenary curve is, strictly speaking, discontinuous at TDP, being zero at the left (on the bottom) and equal to q/T_0, where q is the immersed weigth per unit length. The effect of flexural stiffness is to provide a smooth transition (although abrupt) between this two values, shifting to the left, by an ammount of λ, the actual TDP.
Equation (1) is essential in the analysis of fatigue due to slow-drift motions, when a large variation of the TDP position is expected, mainly under taut conditions. In such situations, the TDP can be assumed to have a quasi-static displacement, foward and back, on the bottom. Equation (1) apllies around the "instantaneous" TDP position, showing that if such a displacement is of order λ, the curvature varies between zero and $\chi_0(s)$, certainly a significant value as far as fatigue is concerned. Generalization of equation (1) for the dynamic problem is not a straightforward task, as the dynamic boundary condition at TDP, of unilateral contact type, must be analyzed first.

A similar result can be derived for the flex-joint vicinity, at the top end. Let $\theta_0(l)$ be the static equilibrium angle with respect to the horizontal at top, correponding to the exact catenary solution ($EJ = 0$) and θ_F be the angle of the flexible-joint axis. Then, local analysis and boundary layer technique lead to (Pesce, Aranha & Martins, 1994)

$$\chi_{f,0}(s) = \chi_0(s) - \frac{K_F}{EJ + K_F\lambda}(\theta_0(l) - \theta_F)e^{-(s-l)/\lambda}, \quad (2)$$

for the static curvature $\chi_{f,0}(s)$ in the vicinity of the top end..In equation (2) K_F is the flexural-spring constant modeling the flexible joint and, now, $\lambda = \sqrt{EJ/T_0(l)}$ is the (local) "flexural length" at top end ($s = l$). So, the static curvature is basically given by the exact catenary solution far away from the flexible-joint. At the very top we have $\chi_0(l) = 0$, by definition, and curvature is proportional to flexural stiffness of the flexible-joint. For our typical 10" SCR, in 1000m deep water ($EJ \approx 25000 kNm^2$), we get $T_0(l) \approx 1000 kN$. If the flexible-joint flexural stiffness is taken to be $K_F \approx 570 kNm/rad$ ($10 kNm/$degree), then $\lambda \approx 5m$ and $K_F\lambda/EJ \approx 0.12$ .. So an angle deviation of order 10 degrees would cause a bending deformation $\varepsilon_F(l) = \chi_{F,0}(l)R \approx 0.5\times10^{-3}$, corresponding to circa 25% of yielding deformation.

Equation (2) can be directly applied to the dynamic problem, by just substituting $\Theta(l,t) = \theta_0(l) + \alpha(l,t)$, computed from any computer code where catenary dynamics is assumed, in place of $\theta_0(l)$, resulting

$$\chi_{f,0}(s,t) = \chi_0(s) - \frac{K_F}{EJ + K_F\lambda}(\Theta(l,t) - \theta_F)e^{-(s-l)/\lambda} \quad ,(2.a)$$

The point to be emphasized here is that SCR dynamics in deep water can be said to be basically governed by catenary equations, bending stiffness effect being of a local nature. Neverthless, flexural rigidity will be significant in the dynamic global response for high-order vibration modes, whenever $\lambda_n/\lambda \cong O(1)$, being λ_n the typical wave-length scale for the mode n, and λ the "flexural length" at top end.

3.2 Boundary Condition at TDP

A proper definition for the dynamic boundary condition at TDP is essential for design purposes, since in this region bending stresses proved to be of great importance in either extreme load conditions or in fatigue analysis. The reasons for studying the TDP dynamics closely arise from two distinct motivations.

On one hand, the purpose is to save time in fatigue analysis, when the dynamic response to a great number of mild loading conditions must be determined. If computer codes based on linear (frequency-domain) models are used, instead of full non-linear (time domain) simulation programs, the question that could be raised is: to what extent would be the results reliable? Usually, such models consider the TDP as invariant in time, either by applying a simple hinged end condition or an elastic (flexural) support. If the first condition is assumed, besides variation of the TDP, bending moment is lost. Aymptotic solutions must then be employed in order to correct the results properly, including TDP's variation with time and the dynamics of that part of the line that lies on the bottom. This first type of condition was thoroughly analysed (Aranha et al., 1995), the main results being summarized below. If the second type of boundary condition is taken, the resulting bending moment must be corrected to incorporate the TDP's variation with time.

On the other hand, *analysis performed by the use of different non-linear time domain simulation computer codes*, in a number of mild environmental conditions, for fatigue prediction purposes , - when bending stresses are relatively small -, have shown that the computed *dynamic bending moment* near the TDP can be more than twice the value determined in the nearby region, outside the *boundary-layer*. This result is, at least qualitatively, in accordance to the "boundary-layer" model, addressed in section 3.3. However, the rms values for bending moment got from non-linear codes are somewhat larger. Such a behavior was firstly thought to be of a physical nature, due to some nonlinear response related to the TDP variation, as for example some impact load on the bottom. This is not the fact, however (see below), and then it was shown that usual discrete models are not able to compute *curvature variations* near TDP properly, even if mesh is refined, numerical convergence being thus assured. As a matter of fact, this ill-behavior is caused by a dynamic-contact force that arises on the discrete mass element that represents the instantaneous point of contact with soil (instantaneous TDP). Although this force goes to zero as discretization size goes, the moment it causes does not, resulting in a *small* but *finite value*, proportional to the static bending moment. In extreme loading conditions this "spurious" numerical value is

neglectable, but not in mild situations, when fatigue is concerned. Remember that in usual S-N curves, accumulated damage increases exponentially with stress amplitude. If API-XL50 steel is taken as an example, this exponent is 4.38, therefore increasing the damage by circa 20, if the stress amplitude is duplicated. This last point will not be mathematically worked out in the present paper.

We then start summarizing catenary local dynamic analysis close to TDP ($x \approx s$). Following Aranha et al., 1995, after Triantafyllou et al., 1985, let the origin O be placed on the exact static catenary TDP. If $z = Z(x,t)$ defines the dynamic configuration in the vicinity of O and $x = x_0(t)$ denotes the instantaneous TDP, then $Z(x_o(t),t) \equiv 0$ and

$$\frac{dZ}{dt}(x_0(t),t) = \frac{\partial Z}{\partial t}(x_0(t),t) + \dot{x}_o(t)\frac{\partial Z}{\partial x}(x_0(t),t) \equiv 0 \quad (3)$$

Also, as shown by Triantafyllou et al., 1985, neglecting dynamic tension $\tau(t)$ compared to the static value T_o,, it follows

$$\left(\dot{x}_0(t) - c_0^{\,2}\right)\frac{\partial Z}{\partial x}(x_0(t),t) = \frac{F_l(t)}{(m+m_a)} \quad , \quad (4)$$

showing that impact force ($F_l(t) > 0$) on the bottom will occurr *only if* $\dot{x}_0 > c_0$, being $c_0 = \sqrt{T_0/(m+m_a)}$ the local wave-velocity traversing the cable, a rather intuitive result.

For our typical 10"-SCR in 1000m deep water, $c_0 \approx 30 - 70 m/s$, and so $\dot{x}_0 << c_0$, in general.

As a matter of fact it is shown that $(\dot{x}_0/c_0)^2 \approx (1/2)\left((m+m_a)/(m-m_a)\right)\cos\bar{\theta}(\omega^2 A/g)(A/h) << 1$, (Aranha et al., 1995), unless A, the amplitude of motion at top end, *is large enough* and $\bar{\theta}$, the average angle along the line, is close to one (taut line). Under the non-impact force condition it then follows that $\partial Z/\partial x(x_0(t),t) \equiv 0$ and $\partial Z/\partial t(x_0(t),t) \equiv 0$, conditions of instantaneous horizontal tangence and vertical zero-velocity, respectively. It means the riser lies on (rises from) the bottom smoothly. We can think of an instantaneous touchdown point that, in analogy with the instantaneous center of rotation in the plane motion of a rigid body, has zero velocity but non-zero acceleration, now given by $\partial^2 Z/\partial t^2(x_0(t),t) = \dot{x}_0^{\,2}\,\partial^2 Z/\partial x^2(x_0(t),t)$.

Expanding $Z(x_o(t),t) \equiv 0$ and $\partial Z/\partial x(x_0(t),t) \equiv 0$ in Taylor Series, around the *static TDP* ($x = 0$), it then follows, with an error of order $(\chi_0(0)x_0)^2$, that $Z(0,t) = 0$, meaning that the *"static TDP can be considered as an articulation for the dynamic problem"* (Aranha et al., 1995). It follows also that as the angular displacement $\alpha(0,t) \equiv \partial Z/\partial x(0,t)$ at the *static TDP* ($x = 0$), is in general a non-zero value, the excursion of TDP can be evaluated as $x_0(t) \cong -(T_0(0)/q)\alpha(0,t)$. In other words, if $Z(0,t) = 0$ is assumed in the linear frequency-domain solution, $\alpha(0,t)$ being thus determined, then the instantaneous position for the actual TDP can be calculated.

The above analysis is, of course, particularly valid in mild load conditions but can be used as well in extreme loading situations, whenever $\dot{x}_0 << c_0$, what in general will take place if the riser is not so tight.

3.3 Dynamic Curvature in the Vicinity of TDP

As shown with details in Aranha et al., 1995, from the dynamic equilibrium of the catenary equation a local analysis around TDP gives us, with an error of order $q(\dot{x}_0/c_0)^2$,

$$T_0(0)\chi(0,t) + \frac{q}{T_0(0)}\tau(0,t) + \tau(0,t)\chi(0,t) = 0, \quad (5)$$

where $\Theta(s,t) = \theta_0(s) + \alpha(s,t)$ is defined as the total dynamic angle with the horizontal plane; $\alpha(s,t)$ represents the dynamic deviation from the static catenary solution $\theta_0(s,t)$; $T(s,t) = T_0(s) + \tau(s,t)$ for the total tension and $\chi(s,t)$ is the dynamic curvature.

Observing then, from experiments and time domain non-linear simulations results, that dynamic tension, under harmonic excitation with frequency ω can be written as $\tau(s,t) = \langle\tau(s)\rangle + \tau_0(s)\cos\omega t + \ldots$, and, from (5), that curvature and tension are out-of-phase by a factor of π (at least in leading-order), the following result was derived , valid in the vicinity of TDP

$$\chi(t) = \chi_0\left[1 - \frac{2(\tau_0/T_0)}{1+\sqrt{1+2(\tau_0/T_0)^2}}\cos\omega t\right], \quad (6)$$

where χ_0 is the static catenary curvature and dependence on s was dropped since the result is concerned with a local analysis.

The point to be emphasized here is that once the static catenary solution is known and dynamic tension amplitude is determined, by means of any computer code, particularly by a linear frequency-domain linear one, the curvature at TDP is promptly calculated. As a matter of fact, τ_0 is practically constant along the riser span, and can be determined from asymptotic analysis, by a simple algebraic formula given in terms of static solution, as shown in Aranha et al., 1993.

The above result applies to the local catenary dynamics. If the *local bending stiffness effect is included*, the following result was derived for the total dynamic curvature, in the vicinity of TDP

$$\chi_f(s,t) = H(s - x_0(t) + \lambda)\left(1 - e^{-(s-x_0(t)+\lambda)}\right)\chi(t), \quad (7)$$

where $H(\circ)$is the Heavyside Function, $x_F(t) = x_0(t) - \lambda$ indicates the instantaneous position of TDP and $\chi(t)$ can be given by (6). So, only we need is to solve the static and the linear frequency-domain problems for the standard catenary equations and bending moment at TDP can be determined. Appendix B presents some examples, showing good agreement between asymptotic solutions and non-linear time simulation results.

4. EXAMPLES AND DISCUSSION

The purpose of the present section is to illustrate the overall design procedure through the presentation of some numerical results concerning a preliminary analysis performed on a SCR in 910m deep water.

4.1 General Data

Most of the results presented as examples refer to a 8"5/8-diameter SCR, for gas exportation, in 910m deep water. The FPS is a semi-submersible platform. The total length is taken to be 5000m, the bottom to be rigid, the friction coefficient as 0.4, the drag coefficient is assumed to be $C_D = 1.1$.

For this case study steps 1 to 5 described in the flowchart (Figure 1), were performed once, i.e., *only the first cycle of design has been accomplished.*

Additionally, a 10"3/4 and a 12"3/4 SCR, have also been analysed, in order to exemplify how diameter, thickness and depth modify some main conclusions. Table 1 shows some relevant data. Static solution and related parameters refer to the neutral position (no current or waves). Notice that neutral configuration was defined according to the procedure described in step 2, so predicting a factor of two for dynamic overloading in the NEAR situation, here assumed to be 100 m from neutral equilibrium. Notice also that, the angle of the riser with respect to vertical is large (~32.4 degrees), if compared to standard flexible-risers solution or even with Auger SCR. As pointed out earlier, however, in that case motions at top are much smaller, either for wave-frequency or slow-drift ones. Also to be noticed the rather large value for tension at top. The "flexural length" λ at TDP is of order 7m, a small value if compared to the suspended length of 1625m, as expected.

Table 1 ***Riser's general data and parameters.***

	RISER 12"3/4	RISER 8"5/8
h	575 m	910 m
D	0.3238 m	0.2191 m
D/t	18.52	17.25
q	0.471 kN/m	0.256 kN/m
EJ	41485 kN m^2	9241 kN m^2
EA	3.53x10^6 kN	2x10^6 kN
x_B	4560 m	4650 m
z_B	565 m	900 m
l	1050 m	1625 m
θ_B	56.9^0	57.6^0
T_B	568 kN	490kN
T_0	310 kN	261kN
c_0	37.9m/s	38.7m/s
λ	11.6m	6.0m

4.2 Extreme Loading Conditions and Fatigue Analysis for the 8"5/8 SCR

A full non-linear time domain simulation code was used for analysis concerning extreme loading conditions and for evaluating fatigue due to first-order motions imposed by the FPS to the riser. Table 2 presents the extreme wave conditions as well as nine distinct wave conditions used in evaluating fatigue.

Table 2. ***Seastate Conditions & Radius and Period of Circular Motion imposed to the Top End. SCR - 8"5/8***

SEA STATE	H_S (m)	T_M (s)	A (m)	P(s)	p(%)
1	0,75	5,24	0.07	7.08	2,3
2	1,25	5,27	0.12	7.11	25,6
3	1,75	5,77	0.20	7.74	38,9
4	2,25	6,26	0.32	8.41	19,6
5	2,75	6,89	0.47	9.23	8,8
6	3,25	7,72	0.70	10.16	3,2
7	3,75	7,89	0.84	10.33	0,8
8	4,25	8,20	1.02	10.64	0,6
9	4,75	9,00	1.31	11.41	0,2
100-YEARS	7,6	9,2	3.5	10.9	-

Pierson-Moskowitz Spectrum was assumed. As the mentioned computer code considers only regular wave and harmonic input, an equivalent circular motion was calculated from FPS's RAO and imposed to the riser top end, for each sea state, by means of standard energy spectrum techniques

Table 3 ***Current Profiles (m/s); Direction: FAR; SCR - 8"5/8***

z (m)	1 year	10 years	100 years	directn	α (°)
-5	1.09	1.40	1.71	SW	0
-20	1.09	1.43	1.77	SW	0
-40	1.04	1.40	1.75	SW	0
-60	1.03	1.40	1.78	SW	0
-80	0.99	1.37	1.75	SW	0
-100	0.89	1.24	1.58	S	-45
-150	0.73	1.02	1.30	S	-45
-200	0.53	0.73	0.93	S	-45
-250	0.40	0.57	0.73	S	-45
-300	0.29	0.42	0.55	NE	180
-400	0.46	0.63	0.80	NE	180
-500	0.49	0.67	0.84	NE	180
-600	0.42	0.57	0.73	NE	180
-910	0.42	0.57	0.73	NE	180

Table 4 ***Current Profiles (m/s);Direction: NEAR. SCR - 8"5/8***

z (m)	1 year	10 years	100 years	directn	α (°)
-5	0.71	0.83	0.92	NE	180
-20	0.59	0.69	0.78	NE	180
-40	0.47	0.55	0.61	NE	180
-60	0.75	0.89	1.01	NE	180
-80	0.89	1.08	1.22	NE	180
-100	0.90	1.10	1.25	NE	180
-150	0.94	1.17	1.34	NE	180
-200	0.98	1.23	1.42	NE	180
-250	0.95	1.21	1.41	NE	180
-300	0.91	1.18	1.40	NE	180
-400	0.87	1.14	1.34	NE	180
-500	0.75	0.94	1.03	NE	180
-600	0.72	0.90	1.03	NE	180
-910	0.72	0.90	1.03	NE	180

For the extreme conditions the amplitude of equivalent circular motion was taken to be $A_B = 3.7 m_0^{1/2}$, corresponding to the maximum value in a three-hour storm, where m_0 is the zero-order moment calculated from the motion-spectrum. For the first-order motion fatigue analysis the motion amplitude at the top end was taken to be $P_B = \sqrt{2} m_0^{1/2}$, with period $(m_0/m_2)^{1/2}$.

Tables 3 and 4 present the current profiles. The angle α gives the velocity direction with respect to the catenary plane, positive clockwise if seen from above and zero towads the FPS. The 1-year return period current was used for fatigue evaluation due to wave-frequency motions.
Table 5 presents FPS offsets in extreme conditions and in average operational situations corresponding to the annual storm.

Table 5. ***FPS Off-set Positions (m) - (from neutral position).***

	Oper.	Extreme
Near (m)	-32	-100
Far (m)	+64	+100

Table 6 shows a summary of extreme response values, corresponding to four environmental conditions. CC stands for Centenary Current; DC for Decenary; CW for Centenary Wave; DW for Decenary. ε is deformation; $\phi = \pi/2 - \theta$ designates angle at top with respect to vertical. Notice that no flexible-joint is considered in the results presented in this table. From equation (2.a), however, the maximum value for the flexible-joint flexural stiffness can be evaluated. In fact, let ε_{adm} be the maximum admissible deformation, usually taken as $0.7\varepsilon_y = 1.4 \times 10^{-3}$, then the maximum K_F will be given by the minimum value satisfying equation (8) below, for all extreme conditions.

$$K_F \le \frac{EJ\left(\varepsilon_{adm} - \frac{T_{max}(l)}{EA}\right)}{R\Delta\theta - \lambda\left(\varepsilon_{adm} - \frac{T_{max}(l)}{EA}\right)}; \quad \Delta\theta = \max\left|\theta - \theta_F\right|_{condition}, \quad (8)$$

In this case, condition FAR-DCCW gives the smallest value for K_F at top, resulting in $\lambda_{min} = 2.33m$, $\Delta\theta = 34.4^o$ and $K_F \le 1.05 kNm/^o$. Just for comparison purposes condition FAR-CCDW gives $\lambda_{min} = 2.45m$, $\Delta\theta = 27.2^o$ and $K_F \le 1.65 kNm/^o$. Correcting, then, the angular displacement at the flexible-joint we get $\Delta\theta_F = (1 + K_F\lambda/EJ)^{-1}\Delta\theta \cong \Delta\theta$, in this case.

Table 6 ***SCR 8"5/8; h=910 m***

Condition	Point	M_{max} (kNm)	ε/εy (%) bendg	T_{max} (kN)	ε/εy (%) tensn	ϕ_{min} (°)	ϕ_{max} (°)	ϕ_{avg} (°)
NEAR-DCCW	TDP	79,9	46	476,5	14	7,7	51,1	30,9
NEAR-CCDW	TDP	99,3	59	307,5	9	17,8	50,9	34,3
FAR-DCCW	TOP	-	-	1695,1	49	25,0	56,8	42,0
FAR-CCDW	TOP	-	-	1539,5	44	28,8	49,6	40,1

Table 7 shows a summary of fatigue evaluation computed in the first cycle of design-spiral, step 4 of design flowchart. Standard Palmgren-Miner rule have been adopted, API-5LX60 S-N curve being used,

$$N = 2 \times 10^6 \left(\frac{14.5 ksi}{\Delta\sigma}\right)^{4.38}$$

A number of simplyfying assumptions have been assumed in this first cycle of design. Three main sources of fatigue have been taken: *wave-frequency loading*, *FPS slow-drift motions* and *VIV*. Accumulated damages per year, corresponding to each excitation source, were computed independently and then summed up. As can be observed, wave-frequency range loading appears to be, at least in this case, the major source of fatigue. This is not always the case, however, as exemplified at the end of this section, taking a 12"3/4-SCR in 575 m deep water

Table 7. ***Fatigue Evaluation. SCR - 8"5/8; h=910m***

EXCITATION	POINT	FATIGUE LIFE (years)
wave-freq. range	near TDP	317
slow-drift range	near TDP	9455
VIV	spanwise	1019729
Combined	near TDP	306

For the loading in the wave-frequency range, associated to first-order motions imposed to the top end by FPS and to direct action of waves along the riser, nine distinct sea states were considered and weighted accordingly (see table 2). Near- and Far-operational offsets and the 1-year return period current profile was taken, in the safe side.

For the *slow-drift motion fatigue*, a non-standard, but otherwise safe criterion was adopted, since we deal with the preliminary analysis. It was assumed that slow drift motion imposed by FPS to the top end was large enough to make the TDP be displaced, back and foward, a distance greater than the corresponding "flexural length" λ, for each offset position. This assumption corresponds to take a curvature variation at TDP equal to the static equilibrium curvature at this point, as the pipe lays down and rises from the bottom. It was also assumed that slow-drift oscillations is a narrow-band spectrum process, in such a way as to take the significant period of oscillation as the natural period of the moored system.

Table 8. ***Slow-drift Fatigue at TDP. SCR-8"5/8***

OFF (m).	l (m)	T_0 (kN)	λ (m)	$\frac{\Delta x_0}{\Delta U}$	ΔU_λ (m)	p (%)	$\frac{dmg}{year}$	$\frac{wdmg}{year}$
-100	1185	48	13.9	1.55	8.9	0.0027	0.167	4.6E-6
-32	1450	169	7.4	2.86	2.6	0.274	6.7E-4	1.8E-6
0	1625	261	5.9	3.84	1.6	99.447	1.0E-4	9.9E-5
+64	1950	427	4.7	5.96	0.8	0.274	1.2E-5	3.2E-8
+100	2175	545	4.1	7.65	0.5	0.0027	4.0E-6	0.1E-9
						ACC.DMG/YEAR		1.06E-04
						FATIGUE-LIFE		9455 years

Table 8 shows, as an example, the computation for 5 distinct FPS offset positions. Most of time the system is supposed to oscillate around the neutral position. $\Delta x_0/\Delta U$ is the amplification factor for TDP variation on the bottom due to a horizontal (in-plane) oscillation ΔU imposed to the top end. ΔU_λ denotes the slow-drift amplitude corresponding to $\Delta x_0 = \lambda$.
The reason for such a simple approach is to show that, usually, slow-drift oscillations will cause a TDP variation larger than the "flexural-length", making this kind of excitation a major source of fatigue. During further cycles of design spiral, of course, slow-drift fatigue evaluation must be

refined. A larger number of sea-states and corresponding offsets should be considered, as well accurate computation of slow-drift motions must be carried on.

For the VIV fatigue analysis Iwan's model, properly adapted, was used (see Appendix A). A linear frequency-domain program was run for determining the eigen-modes.Table 9 shows current profiles used, stratified according five depth ranges. It is also presented the corresponding probability of occurrence. For simplicity, it was assumed that directions are such that vibration modes in the catenary-plane are always excited. Extreme current conditions were not analysed, during this first cycle of design. Numbers in brackets indicate the highest mode that is excited in that velocity range. As can be observed, up to mode number 24 can be excited by these current profiles. Table 10 shows the accumulated damage per year, for each mode, if excited permanently and along the whole span. The "amplification factor" F_n was then applied, as shown in Appendix A, in order to consider partial excitation along the suspended length. Notice that two columns are shown for the periods T_n and for the damages D_n. The former ones were computed assuming purely sinusoidal modes. No major differences can be seen.

Table 9 Current Profiles for VIV Fatigue Analysis. SCR - 8"5/8. Neutral Offset

(n) is the highest excited mode

PROFILE	DEPTH RANGE (m)					
	1	2	3	4	5	P
	0-182	182-364	364-546	546-728	728-910	(%)
1	0.140 (3)	0.135 (3)	0.182 (4)	0.153 (3)	0.153 (3)	0.1
2	0.182 (4)	0.223 (5)	0.248 (6)	0.282 (7)	0.279 (7)	0.6
3	0.206 (5)	0.146 (3)	0.175 (4)	0.218 (5)	0.221 (5)	3.8
4	0.234 (6)	0.133 (3)	0.169 (4)	0.194 (4)	0.195 (4)	12.0
5	0.284 (7)	0.137 (3)	0.179 (4)	0.194 (4)	0.190 (4)	18.0
6	0.360 (9)	0.145 (3)	0.225 (5)	0.192 (4)	0.188 (4)	20.0
7	0.434 (12)	0.167 (4)	0.157 (3)	0.187 (4)	0.188 (4)	18.0
8	0.487 (14)	0.165 (4)	0.199 (5)	0.173 (4)	0.174 (4)	12.0
9	0.545 (16)	0.174 (4)	0.143 (3)	0.166 (4)	0.168 (4)	7.2
10	0.530 (15)	0.149 (3)	0.121 (2)	0.183 (4)	0.190 (4)	5.0
11	0.550 (16)	0.135 (3)	0.124 (2)	0.169 (4)	0.173 (4)	2.7
12	0.615 (18)	0.162 (3)	0.133 (3)	0.148 (3)	0.146 (3)	0.7
13	0.720 (20)	0.169 (4)	0.153 (3)	0.203 (5)	0.210 (5)	0.04
14	0.812 (24)	0.192 (4)	0.188 (4)	0.186 (4)	0.190 (4)	0.04

Table 10 ***Accumulated Damage per Year Due to VIV. SCR - 8"5/8;excitation over the whole length***

Mode	Tn (seg) (*)	Tn (seg) (**)	Un (m/s)	0.8*Un (m/s)	2.0 Un (m/s)	Nn (CYCLES)	Dn (*) AC. DAMAGE PER YEAR	Dn (**) AC. DAMAGE PER YEAR
1	30.187	30.597	0.077	0.062	0.155	2.6776E+18	3.9016E-13	3.8493E-13
2	20.125	20.149	0.118	0.094	0.235	7.6768E+16	2.0412E-11	2.0388E-11
3	15.094	14.461	0.164	0.131	0.328	6.1762E+15	3.383E-10	3.5309E-10
4	12.075	11.629	0.204	0.163	0.407	8.7455E+14	2.9863E-09	3.1008E-09
5	10.062	9.552	0.248	0.198	0.496	1.7708E+14	1.7699E-08	1.8645E-08
6	8.625	8.226	0.288	0.230	0.576	4.5889E+13	7.968E-08	8.3544E-08
7	7.547	7.143	0.332	0.265	0.663	1.4246E+13	2.9333E-07	3.0991E-07
8	6.708	6.376	0.372	0.297	0.743	5.0769E+12	9.2597E-07	9.7422E-07
9	6.037	5.708	0.415	0.332	0.830	2.0173E+12	2.5894E-06	2.7388E-06
10	5.489	5.213	0.455	0.364	0.909	8.7531E+11	6.5642E-06	6.9112E-06
11	5.031	4.756	0.498	0.399	0.996	4.0845E+11	1.5346E-05	1.6234E-05
12	4.644	4.423	0.536	0.429	1.071	2.0259E+11	3.3518E-05	3.5194E-05
13	4.312	4.092	0.579	0.463	1.158	1.0585E+11	6.9088E-05	7.281E-05
14	4.025	3.952	0.600	0.480	1.199	5.7837E+10	0.00013547	0.00013797
15	3.773	3.743	0.633	0.506	1.266	3.286E+10	0.00025433	0.0002564
16	3.551	3.554	0.667	0.533	1.333	1.9321E+10	0.00045959	0.00045926
17	3.354	3.34	0.709	0.568	1.419	1.1711E+10	0.00080288	0.00080628
18	3.178	3.166	0.748	0.599	1.497	7292593457	0.0013609	0.00136588
19	3.019	2.994	0.791	0.633	1.583	4653082854	0.00224515	0.00226367
20	2.875	2.848	0.832	0.666	1.664	3034747246	0.00361453	0.00364875
21	2.744	2.711	0.874	0.699	1.748	2019021129	0.00569164	0.00576151
22	2.625	2.59	0.915	0.732	1.830	1367816078	0.00878326	0.00890183
23	2.516	2.477	0.957	0.765	1.913	942134853	0.01330619	0.01351349
24	2.415	2.375	0.998	0.798	1.995	658884167	0.01981921	0.02015273
25	2.322	2.28	1.039	0.831	2.078	467301333	0.02906242	0.02959884

(*) assuming purely sinusoidal modes; (**) modes as determined from modal anlaysis.

4.3 Depth, Diameter and Thickness Influence

Concluding this section, Table 11 shows fatigue life evaluation for the same pipe, 8"5/8- SCR, but now in a 775 m deep water. Slow-drift appears as the major source of fatigue, instead of wave-frequency range motions. As a matter of fact, the pipe links two distinct but similar FPS in the same oil-field, being the deeper at SE side. Obviously current profiles are not the same in both case, neither are the directions of incidence of both current and waves. Stonger currents are now towards the Near-offset, whilst higher waves goes towards the Far-offset position. Neverthless, the results presented in Table 11 serve to indicate that slow-drift motions tend to be more significant, concerning fatigue, as depth decreases. Wave-frequency range motions, on the contrary, are more important in deep waters. Concerning VIV, it should be mentioned that modes up to number 20 are now excited ($l = 1350m$ in neutral offset position), resulting in half the damage compared to the former case.

Table 11. ***Fatigue Evaluation. SCR - 8"5/8 - h=775m***

EXCITATION	POINT	FATIGUE LIFE (years)
wave-freq. range	near TDP	8972
slow-drift range	near TDP	3485
VIV	spanwise	2007584
Combined	near TDP	2506

Table 12. ***Fatigue Evaluation. SCR - 12"3/4 - h=575m***

EXCITATION	POINT	FATIGUE LIFE (years)
wave-freq. range	near TDP	812
slow-drift range	near TDP	249
VIV	spanwise	7410
Combined	near TDP	185

A similar trend seems to be present in table 12, where the 12"3/4-SCR, in 575 m deep water is analysed. Here orientation is pretty similar to the first case (8"5/8 - 910m). Now slow-drift is even more significant for fatigue life, eventhough VIV damage has increased dramatically if compared to the previous cases.

As a final example, Table 13 shows that the ratio diameter/thickness can be important in avoiding dynamic compression under extreme loading conditions. In this example a 10"3/4-diameter SCR was taken, using three different thickness ratio. Total length is 5000m; top end is 9.2m above waterlevel; current was considered for two offset positions (Near & Far); see Table 14. Wave and FPS motions correspond to maximum wave-heigth found in a centenary sea-state ($H_{max} = 14.2m, T = 12s, A_B = 4.05m$). As the purpose is to compare results concerning the tendency to dynamic compression, that must obviously be avoided, a linear frequency-domain program code was used, for simplicity. As compression occurs, strong non-linear responses take place, in general, giving rise to large peaks of bending moment. The linear model is, of course, not able to compute such a behavior. Neverthless, it can predict quite well not only the trend in tension but also the order of magnitude of tension amplitude.

Table 13. ***10"3/4-SCR; 910m; Extreme Loading Conditions; Linear (frequency-domain) Code Used***

	$\frac{D}{t} = 10.75$		$\frac{D}{t} = 14.95$		$\frac{D}{t} = 17.20$	
	NEAR -10%h	**FAR +10%h**	**NEAR -10%h**	**FAR +10%h**	**NEAR -10%h**	**FAR +10%h**
$x_{topo}(m)$	4460	4642	4460	4642	4460	4642
$\phi_{TOP}(°)$	18.2	32.2	20.1	31.9	21.9	31.6
$l(m)$	1196	1687	1186	1690	1178	1692
TDP						
$T_0(kN)$	286.4	1022.2	152.6	592.9	105.1	440.0
$T_{max}(kN)$	609.5	2235.0	445.5	1708.6	408.6	1517.9
$T_{min}(kN)$	-36.6	-190.5	-140.2	-522.7	-198.5	-637.8
$\tau_0(kN)$	323.0	1212.7	292.9	1115.7	303.6	1077.8
τ_0/T_0	1.13	1.19	1.92	1.88	2.89	2.45
TOP END						
$T_0(kN)$	1150.2	1886.3	651.1	1091.4	473.7	808.4
$T_{max}(kN)$	1533.0	3074.4	977.2	2172.2	798.8	1842.0
$T_{min}(kN)$	767.6	699.1	324.9	10.7	148.6	-225.2
$\tau_0(kN)$	382.7	1187.6	326.2	1080.7	325.1	1033.6
τ_0/T_0	0.33	0.630	0.50	0.990	0.69	1.28

As can be observed, tension amplitude is almost the same, either at TDP or at the top end. It should be mentioned that tension amplitude τ_0. resulted practically invariant along the riser span, confirming asymptotic analysis conclusion (see Aranha et al, 1993). The ratio τ_0/T_0, between dynamic amplitude and static tension is, of course larger at TDP, what makes compression to appear first in this region. Concerning thickness, the ratio τ_0/T_0 ***decreases as thickness increases,*** thus avoiding compression, as expected. Neverthless, tension increases dramatically. Notice also that environmental conditions as well as motions imposed are really hard.

Table 14. ***Current Profiles (m/s);(in the catenary plane); 10"3/4 - SCR; 910m***

DEPTH (m)	NEAR	FAR
0	-1.70	1.22
-20	-1.65	1.01
-80	-1.39	0.54
-150	-1.01	0.72
-200	-0.57	0.50
-400	-0.57	0.42
-600	-0.57	0.35
-890	-0.57	0.35
-910	0.0	0.0

5. CONCLUSIONS

Steel Catenary Risers for deep water applications in Semi-Submersible Floating Production Systems still requires further studies. A simple design procedure that accounts for *static analysis, extreme loading conditions response* and *fatigue*, has been described in the present work. Emphasis has been given on the precise evaluation of dynamic bending moment in the vicinity of the Touch-Down Point. Accuracy in bending moment computation is mandatory as accumulated damage increases exponentially with a power of (circa) four with respect to stress amplitude. For this reason, some results have been recovered from previous asymptotic analysis permiting to discuss boundary conditions at TDP, as well the local nature of bending stiffness effect, that is restricted to regions of high curvature or sudden variation of flexural rigidity. The bending moment distribution in the vicinity of the flexible-joint at the top end have been addressed as well.

Through a number of numerical examples, concerning steel pipes for gas exportation suspended by a semi-submersible FPS, it has been found that slow drift-oscillations of the vessel and motions in the wave frequency region are, in general, the primary cause of fatigue damage, but vortex induced vibrations can play a rule as well, depending on depth, current profile and geometric properties of the riser. Usually, slow-drift oscillations will cause a TDP variation larger than the "flexural-length", making this kind of excitation a major source of fatigue. During further cycles of design spiral, of course, slow-drift fatigue evaluation must be refined. A larger number of sea-states and corresponding offsets should be considered, as well accurate computation of slow-drift motions must be carried on.

Response to extreme loading conditions can be of crucial importance as wave-frequency motions imposed to the top by the semi-submersible FPS are relativelly large. In this respect, diameter-to-thickness ratio has been shown as a very important parameter to be optimized in order to balance conflicting behaviors as, for example, maximum value of tension at top, maximum dynamic curvature at TDP and the possibility of dynamic compression along the riser span.

Neverthlees, a number of questions rest to be answered demanding further and deeper studies. Vortex Induced Vibrations on catenary pipes, in varying current profiles (intensity an direction), are not yet properly modeled. Existing codes for non-linear time-domain simulations seem to present some troubles in computing accurately the bending moment in the vicinity of TDP. The concurrent action of wave-frequency motions and slow-drift oscillations in fatigue evaluation demand more research effort. Low-cycle fatigue during storms, as well impact loads on the riser close to sea-surface have to be considered. Dynamic compression and soil-pipe interaction are also topics deserving special attention. Finally design criteria must be discussed and established.

ACKNOWLEDGEMENTS

This work has been partially supported by FAPESP Fundação de Amparo à Pesquisa do Estado de São Paulo, and partially by CNPq, Brazilian National Research Council. We are also indebt to PETROBRAS/DEPRO staff, in particular to Eng. I. Scherer, for providing case studies data.

REFERENCES

Aranha, J.A.P, Pesce, C.P., Martins, C.A. & Andrade, B.L.R. (1993) "Mechanics of Submerged Cables: Asymptotic Solution and Dynamic Tension". *3rd International Offshore & Polar Engineering Conference*, Singapore, Jun. 6-11, 1993; vol. 2, pp.345-356.

Aranha, J.A.P, Martins, C.A. & Pesce, C.P. (1995) "Dynamic Bending Moment at the Touchdown Point of a Steel Catenary Riser: Analytical Approximation and Numerical Results", (submitted).

Irvine, M. (1992) "Local Bending Stress in Cables". *Second International Offshore and Polar Engineering Conference*, San Francisco, 1-19 June, 1992, Proceedings, Vol. 2, pp. 342-345.

Iwan, W. D. & Blevins, R. D. (1974) "A Model for Vortex Induced Oscillation of Structures". *Journal of Applied Mechanics*, September 1974, p.581-586

Iwan, W. D. (1975) "The Vortex Induced Oscillation of Elastic Structural Elements". *Journal of Engineering for Industry*, November 1975, p. 1378-1382.

Iwan, W. D. (1981) "The Vortex-Induced Oscillation of Non-Uniform Structural System". *Journal of Sound and Vibration*, 1981, 79(2), p. 291-301.

Lyons, G. J. e Patel, M. H. (1986) "A Prediction Technique for Vortex Induced Transverse Response of Marine Risers and Tethers". *Journal of Sound and Vibration*, 1986, 111(3), p.467-487.

Martins, C. A. (1989) "Active Damping for Reducing Vortex Induced Vibration in Risers". São Paulo, EPUSP, 1989. 309p. Doctoral Thesis (in portuguese).

Phifer, E.H., Kopp, F., Swanson, R.C., Allen, D.W. & Langner (1994), C.G. "Design and Installation of Auger Steel Catenary Riser". *Offshore Technology Conference*, 26th, Houston, Texas, May 2-5, 1994; pp. 399-408.

Pesce, C.P. Aranha, J.A.P., Martins, C.A. (1994) "Submerged Cables and Pipes in "Catenary" Configuration. Elements for Design & Analysis", *Lecture Notes*, Escola Politécnica, University of São Paulo, 208 pp. (in portuguese).

Triantafyllou, M.S., Bliek, A. &Shin, H"(1985). "Dynamic Analysis as a Tool for Open-Sea Mooring System Design" SNAME *Annual Meeting*, November, 1985, New York, N.Y.

Appendix A - Vortex Induced Vibrations

VIV can be significant in evaluating fatigue. Let $z_n(s) = A_n\varphi_n(s)$ be the dynamic response of the riser, corresponding to vibration mode n. The amplitude A_n is supposed to be small. Then $\varepsilon_n(s) \cong 1/2\, A_n D(d^2\varphi_n/ds^2)$, with D the external diameter, gives the maximum deformation along the riser span. A standard S-N curve can be put in terms of deformation and written as $N_n = a\varepsilon_n^{-b}$, giving the number of cycles to fatigue failure for mode n, under the reponse amplitude A_n, under the assumption that excitation occurs over the whole span. The point here is how to consider properly the fact that the current profile is non-uniform with depth, mode n being thus excited just over a part of the riser. The considerations to be done are somewhat lengthy and out-of-scope for the present work. The results summarized below are extracted from Martins, 1994 and based on the models proposed in the works of Iwan & Blevins, 1974, Iwan 1975, 1981, further extended for non-uniform current profiles by Lyons & Patel, 1986.

As shown in details in Martins, 1989, and Martins,1994, the amplitude A_n, can be written as $A_n = DF_n I_n^{-1/2}$, where I_n is a shape form, given by

$$I_n = \frac{\int_0^l m(s)\varphi_n^4(s)ds}{\int_0^l m(s)\varphi_n^2(s)ds} \qquad \text{(A.1)}$$

and F_n is an amplification factor, defined by Iwan & Blevin, 1975, that depends on modal damping coefficient and on the modal effective mass.

$$\nu_n = \frac{\int_0^l m(s)\varphi_n^2(s)ds}{\int_0^l S_n(s)\varphi_n^2(s)ds} \qquad \text{(A.2)}$$

where $S_n(s)$ is 1 in the parts of the riser under excitation and 0 otherwise.

As shown by Iwan, 1981, the amplification factor F_n has an empirical expression, given by

$$F_n = \frac{1}{1+9{,}60\left(\mu_n\zeta_n^2\right)^{1{,}80}} \qquad \text{(A.3)}$$

where $\mu_r'' = 4\,\nu_n/(\rho\pi D^2)$ is the effective reduced mass for mode n and the modal damping factor ζ_n^s is written

$$\zeta_n^s = \zeta_n^I + \phi_n F_n \tag{A.4}$$

with

$$\phi_n = \frac{2}{3\pi}\frac{\int_0^l c_d\rho_a D^2[1-S_n(s)]|\varphi_n^3(s)|ds}{\left[\int_0^l m(s)\varphi_n^4(s)ds\right]^{1/2}\left[\int_0^L m(s)\varphi_n^2(s)ds\right]^{1/2}} \tag{A.5}$$

and ζ_n^I as the internal structural damping factor. If $\varphi_n(s) \equiv \text{sen}(n\pi s/l)$ is assumed as an approximation for mode n - particularly good for higher-order modes, when fatigue is relevant- , the following results can be derived,

$$I_n = \frac{3}{4};\ \nu_n = m\frac{n}{k} \tag{A.6}$$

where k denotes the number of half-wave lengths excited;

$$\varepsilon_n = A_n\frac{D}{2}\left(\frac{n\pi}{L}\right)^2;\quad A_n = 1{,}15DF_n;\quad N_n = a\left(A_n\frac{D}{2}\left(\frac{n\pi}{L}\right)^2\right)^{-b} \tag{A.7}$$

and so, as a function of (k/n),

$$N_n(k/n) = a\left(1{,}15\frac{D^2}{2}\left(\frac{n\pi}{L}\right)^2\right)^{-b}F_n^{-b}(k/n) \tag{A.8}.$$

Now, if internal structural damping is neglected, then

$$\zeta_n^s = \phi_n F_n;\qquad \phi_n = 0{,}208\frac{c_d\rho_a D^2}{m}\left(1-\frac{k}{n}\right)$$
$$\mu_r''\phi_n = 0{,}291c_d\left(\frac{n}{k}-1\right);\qquad F_n = \frac{1}{1+1{,}04\left[\left(\frac{n}{k}-1\right)F_n\right]^{1{,}80}} \tag{A.9}$$

Table A.1 shows, as a function of k/n, the factor F_n when internal structural damping is neglected and, assuming $b = 4{,}38$, the normalized number of cycles to fatigue $N_n^r = N_n(k/n)/N_n^1$, where N_n^1 corresponds to the number of cycles to fatigue when $k = n$, i.e., when excitation takes place all over the riser.

If internal structural damping is considered the amplification factor F_n will depend on the mass of the riser, but a similar table can be constructed. As an example if a riser with $D = 0.4064m$, $m = 0.254t/m$, $\zeta_n^I = 2\%$, is taken we get the results presented in Table A.2. It should be remembered, however that mode excitation occurs when $4 < v_r < 8$, where $v_r = (v/(f_n D\sin\theta))$ is the reduced velocity, being v the current profile and $\theta(s)$ the angle with the horizontal.

Table A.1 Amplification factor F_n, and normalized number of cycles to fatigue failure N_n^r for $b = 4{,}38$

k/n	F_n	N_n^r
1,0	1,000	1,
0,8	0,930	1,37
0,6	0,764	3,25
0,4	0,565	12,2
0,2	0,347	103,

Table A.2- *Factor F_n and normalized number of cycles to fatigue failure N_n^r for $b = 4{,}38$, $D = 0.4064m$, $m = 0.254t/m$, $\zeta_n^I = 2\%$,*

k/n	F_n	N_n^r
1,0	0,973	1,13
0,8	0,846	2,08
0,6	0,666	5,93
0,4	0,471	27,1
0,2	0,264	341,

Appendix B - Some Examples Concerning Asymptotic Solutions

For the 8"5/8 - SCR in a 910m deep water, response to wave loading corresponding to table 2 of section 4.2 were analysed, but now, for comparison purposes, taking asymptotic, linear an non-linear solutions. Absence of current and the same neutral offset position were assumed for all simulations. Table B.1 shows general data and parameters refering to the neutral condition.

Table B.1. *Mechanical and static riser's parameters.*

	RISER 8"5/8
h	910 m
D	0.2191 m
q	0.26 kN/m
EJ	9241 kN m^2
EA	2x10^6 kN
x_B	4500 m
z_B	900 m
l	1233 m
θ_B	72.2^0
T_B	332 kN
T_0	102 kN
c_0	31 m/s
λ	9.5 m

Refering to Aranha et al., 1993, the dynamic tension can be calculated by means of simple algebraic formula, deduced from asymptotic analysis, given in frequency domain as function of amplitude at top end and depending only on the static solution, through some functions of form, and on damping coefficient. The amplitude for the dynamic tension is given by,

$$\tau_0 = \nu\, EA \frac{A_B}{l + l_e} \quad . \tag{B.1}$$

with

$$\nu = Max\{\nu_1; \nu_2\} \quad , \tag{B.2}$$

where the "quasi-static" solution is given by

$$\nu_1 = \frac{1}{1+J} \quad . \tag{B.3}$$

$$J_n = \frac{T_0}{l}\int_0^l \frac{\theta^n(s)}{T(s)} ds \quad ; \quad n = 0,1,2 \quad ; \tag{B.4}$$

$$\Gamma = I_2^{1/2}\left(\frac{EA}{T_0}\right)^{1/2}\left(\frac{l}{l+l_e}\right)^{1/2} \quad ; \tag{B.5}$$

being l_e the effective length on the soil and

$$J = \frac{K_e}{K_g} = \left(J_2 - \frac{J_1^2}{J_0}\right)\frac{\Gamma^2}{I_2} \quad . \tag{B.6}$$

the ratio between elastic and geometric rigidity. Or the "dynamic solution", for large enough frequencies,

$$\nu_2 = (V_0\Omega)^2\left[1 + 1/(\zeta V_0)^2\right]^{1/2} \quad . \tag{B.7}$$

that depends on,

$$V_0 = \frac{1}{\Omega^2}\left[\frac{\sqrt{(1-\Omega^2/\zeta)^4 + 4\Omega^4} - (1-\Omega^2/\zeta)^2}{2}\right]^{1/2} \quad , \tag{B.8}$$

being

$$\Omega = \pi\frac{\zeta^{1/2}}{\Gamma}\frac{\omega}{\omega_c} \quad , \tag{B.9}$$

the reduced frequency and

$$\omega_c = \frac{\pi}{l}c_0 \tag{B.10}$$

is the "geometric rigidity frequency". The damping coefficient is given by

$$\zeta = \frac{8}{3\pi}\frac{2C_D}{\pi}\frac{m_a}{m+m_a}\frac{A_B}{D}\frac{I_3}{I_2^2} \quad . \tag{B.11}$$

where A_B is the amplitude of circular motion imposed to the top at frequencyω, and I_k are factors of form, dependent on catenary static curvature, given by,

$$I_n = \frac{1}{l}\int_0^l \left(l\frac{d\theta}{ds}(s)\right)^n ds \quad ; \quad n = 2,3. \tag{B.12}$$

Table B.2 shows results concerning the RMS of dynamic tension computed by:

- *asymptotic solution (Aranha et al., 1993)* - (ASYMPTOTIC);
- *linear (frequency-domain) computer code* (LINEAR);
- *full non-linear time-domain simulation program code* (NON-LINEAR).

The agreement is quite good, indeed, even in extreme loading conditions. Dynamic tension resulted, from linear and non-linear codes, essencialy constant all over the riser, as predict by asymptotic analysis. Moreover, static tension (102kN) and static bending moment (23.4 kNm) at TDP were confirmed by both program codes whithin quite accetable error.

Table B.2. *Tension(kN) RMS for the SCR-8"5/8*

SEA-STATE	ASYMPTOTIC	LINEAR	NON-LINEAR
1	2.2	2.0	1.9
2	3.7	3.3	3.5
3	5.2	4.6	5.1
4	7.3	6.8	7.4
5	9.3	8.9	9.9
6	12.6	12.8	13.9
7	15.6	16.2	17.3
8	19.5	20.6	21.8
9	25.0	25.0	28.4
100-YEAR	161.1	173.5	155.6

Table B.3. *Bending Moment(kNm) RMS in the vicinity of TDP* ($s / \lambda \approx 1$), *for the 8"5/8 SCR*

SEA-STATE	ASYMPTOTIC	LINEAR	NON-LINEAR
1	0.5	0.4	0.4
2	0.8	0.8	0.6
3	1.1	1.2	0.9
4	1.7	1.5	1.4
5	2.1	2.1	1.8
6	2.9	2.9	2.5
7	3.5	3.7	3.1
8	4.3	4.6	3.8
9	5.4	5.4	4.8
100-YEAR	17.2	17.5	15.3

Table B.3 presents some results concerning bending moment RMS *close to* TDP ($s / \lambda \approx 1$) computed by:

- *asymptotic solution* (equation (6), section 3, and dynamic tension by asymptotic solution) - (ASYMPTOTIC)
- *linear (frequency-domain) computer code* (equation (6) incorporated in the linear code) (LINEAR);
- *full non-linear time-domain simulation program code* (NON-LINEAR)

The results compare well with each other. It should be mentioned that a somewath gross mesh was utilized in the non-linear simulation, close to TDP (15m), value that is greater than the "flexural-length" (9.5m). On the other hand, the dynamic-linear code runs over a static solution determined by a rather robust auto-adaptative mesh sizing algoritm. The effect of the "flexural boundary-layer" is not shown in table B.3 (see Aranha et al., 1995).